Astronomy and Computing 44 (2023) 100729

Contents lists available at ScienceDirect

Astronomy and Computing

journal homepage: www.elsevier.com/locate/ascom

Full length article

Solar Hα image interference fringes removal based on stationary wavelet deep neural network

Kui Wu

Faculty of Information Engineering and Automation, Kunming University of Science and Technology, Kunming 650500, China

ARTICLE INFO

Article history:
Received 2 March 2023
Accepted 13 June 2023
Available online 19 June 2023

Keywords:
Neural network
Interference fringe
Wavelet transform
Image pyramid

ABSTRACT

The solar Hα images acquired by the Goode Solar Telescope (GST) at the Big Bear Solar Observatory (BBSO) are superimposed by interference fringes. These fringes degrade the image quality and seriously affect later research that uses these data. To remove the interference fringes in Hα images, this paper proposed a method combining stationary wavelet deep convolutional neural network (SWT-CNN) and image pyramid. First, the image pyramid was used to downsample the fringe image, which sped up the neural network training speed. Then, SWT-CNN used the difference between fringe image and fringe-free image to remove the interference fringe. Finally, the image size was recovered by the Laplacian pyramid. The experimental results show that our method can effectively remove the interference fringes in Hα images and preserve the solar structure.

1. Introduction

Hα images are important for astronomers because they can be used to observe optical flares, among other things. The solar Hα images obtained by the GST contain interference fringes due to the observation equipment. These Hα images were taken by The Visible Imaging Spectrometer (VIS) of GST. VIS is based on a single Fabry–Pérot etalon. The light of the Fabry–Perot interferometer is very monochromatic and easily forms interference fringes between the membranes of the camera. These interference fringes will show up when seeing is not good. Fig. 1 shows an Hα image with interference fringes. There are two kinds of stripes in the image, one is a horizontal stripe, which is a fixed pattern noise caused by CMOS. Another type of fringe that is at a 30 deg from the horizontal line is the interference fringe. At present, there are many effective methods to remove the fixed mode noise, but the method to remove the interference fringe is lacking. Interference fringes seriously affect the later research that uses these data. Therefore, many researchers have begun to study the removal of interference fringes in astronomical images.

He et al. (2014) removed the stripe noise in Hα images by adaptive wavelet transform (AWT) and Gaussian low-pass filtering. Gaussian low-pass filtering only removes the high-frequency noise, not the low-frequency noise, and makes the image too smooth while removing the fringe noise. Zheng et al. (2016) proposed a method based on least squares support vector machine to remove streaks from Hα images of the Huairou Solar Observatory.

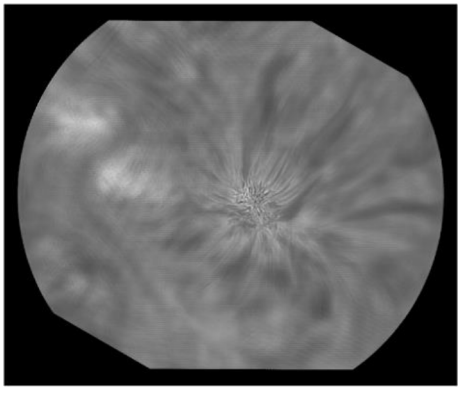

Fig. 1. An Hα image with interference fringes that was obtained on 2014 August 13 at 17:52:01 UT.

Wang et al. (2016) used frequency-domain filtering and spatial-domain filtering to extract interference fringes in NVST data. SVM, frequency-domain filtering and spatial-domain filtering had the same deficiency as Gaussian low-pass filtering. Cai et al. (2018) and Liu et al. (2020) applied principal component analysis (PCA) in the spatial and frequency domains to remove interference fringes in NVST data, respectively. The NVST fringe belongs to the high-frequency part, while the GST fringe not only has the low-frequency part but also the high-frequency part. PCA cannot effectively separate the fringes and solar structure information. Li et al. (2019) proposed a method for removing interference fringes

E-mail addresses: jacobwu96@qq.com, jacob_wu@stu.kust.edu.cn.

https://doi.org/10.1016/j.ascom.2023.100729
2213-1337/

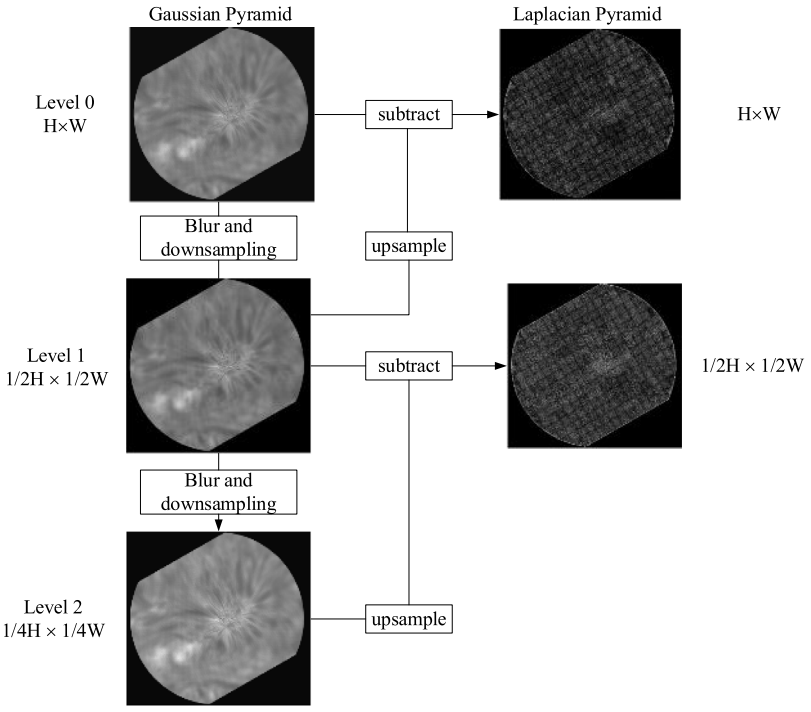

Fig. 2. Schematic diagram of image pyramid. The Hα image is downsampled twice, and the image size becomes a quarter of the original size. And there is no obvious fringe structure in the Laplacian image.

in NVST images based on multiscale decomposition and adaptive partitioning. The interference fringes in the GST data are almost all over the image. The adaptive segmentation method is not very useful, and Gaussian filtering does not perform well in fringe removing. "Fringes Flat Field" (Liu et al., 2021) is not applicable to speckle reconstruction images. Deep learning methods are also used to remove interference fringes in astronomical images. Li (2021) improved DnCNN and applied it to remove interference fringes in NVST data. DnCNN is not effective in removing high-intensity interference fringes, and the solar structure information retention performance is not good. Inspired by transform domain neural networks in image denoising (Gao et al., 2018; Guan et al., 2019; Liu et al., 2022; Kim et al., 2022) and image pyramid (Adelson et al., 1983; Burt and Adelson, 1983) in image processing, we proposed a method combining image pyramid and SWT-CNN. The image pyramid is used to sped up the training speed of the neural network, and the SWT-CNN uses the difference between the fringe image and fringe-free image in the frequency domain to remove the interference fringes while retaining the solar structure information.

This paper is organized as follows: in Section 2, we introduce the GST observation data; Section 3 introduces the techniques used in this paper; In Section 4 we introduce the dataset and the network structure; the experimental results are analyzed in Section 5; and Section 6 concludes the paper's work.

2. Observation

GST operates the Broadband Filter Imager (BFI), Visible Imaging Spectrometer (VIS), and Near Infrared Imaging Spectropolarimeter (NIRIS). The Hα data were taken with the NST Visible Imaging Spectrometer (VIS). VIS is based on a single Fabry–Pérot etalon that produces a narrow 0.08 Å bandpass over a 75"×64" FOV. This tunable filter operates within a 5500–7000 Å range and the image scale is 0.029"/pixel at Hα 6563 Å line.

The data used in this paper are Hα images acquired by BBSO. The fringe images were observed on August 13, 2014, with a total of 1794 images. The fringe-free images are from the period of October 2 to November 6, 2014, with a total of 5000 images.

3. Theory

3.1. Image pyramid

Image pyramid is a group of subimages of the same image with different resolutions, which is generated by continuously downsampling the original image, that is, generating low-resolution images from high-resolution images (Adelson et al., 1983; Burt and Adelson, 1983). There are two types of image pyramids, namely Gaussian pyramid and Laplacian pyramid. The process of the image pyramid algorithm is shown in Fig. 2. The Gaussian pyramid is obtained by smoothing the image once and then downsampling the smoothed image to obtain an image that is half the size of the original image. The process is repeated to obtain a smaller image. The image information lost in the downsampling process constitutes the Laplacian pyramid. The use of Laplacian pyramid can reduce the loss of image information when the image is downsampled and then upsampled to recover the image. We added the image pyramid to SWT-CNN to sped up the neural network training speed. We downsample the image twice to reduce the image size without causing loss of fringe structure in the downsampling process. Each time the data was subsampled, the training time was reduced to a quarter of the original time. If the data is downsampled three times, distinct fringe structures appear in the image of the Laplace pyramid. Subsampling twice can effectively accelerate the training speed of the neural network, but will not significantly affect the effect of removing fringe.

3.2. Stationary wavelet transform

Stationary wavelet transform (Nason and Silverman, 1995) is an improvement of discrete wavelet transform (DWT). In discrete wavelet transform, the image must be downsampled. However, SWT does not require downsampling, and the size of the decomposed wavelet coefficient is the same as that of the original image, which can effectively avoid the Gibbs phenomenon caused by

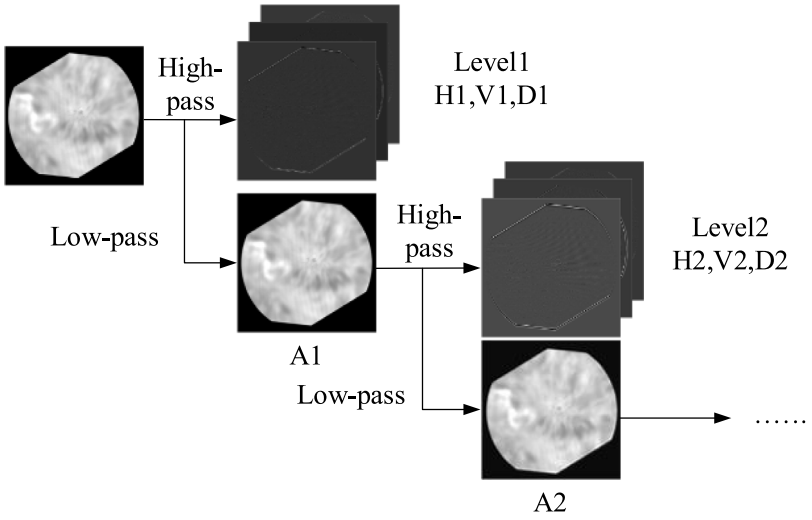

Fig. 3. Schematic diagram of stationary wavelet decomposition. SWT can separate the interference fringe from the solar structure information, so as to reduce the loss when removing the interference fringe.

downsampling. In addition, to remove the interference fringes, the image needs to go through a deep level of wavelet decomposition. If the image is downsampled many times, the wavelet coefficient image will become very small, and it is difficult to distinguish the noise from the image part, which is not conducive to removing the fringes. The stationary wavelet transform decomposition formula is as follows:

$$\begin{cases} c_{j,k} = \sum_n h_0^{\uparrow 2j}(n-2k)\, c_{j-1,n} \\ d_{j,k} = \sum_n h_1^{\uparrow 2j}(n-2k)\, d_{j-1,n} \\ h_0 = \langle \varphi_{1,0}, \varphi_{0,k} \rangle \\ h_1 = \langle \psi_{1,0}, \psi_{0,k} \rangle \end{cases} \tag{1}$$

where $c_{j,k}$ is the low-frequency coefficient, $d_{j,k}$ is the high-frequency coefficient, $h_0^{\uparrow 2j}$ and $h_1^{\uparrow 2j}$ represent the insertion of $2^j - 1$ zeros between the two points h_0 and h_1, respectively, φ is the scale function and ψ is the wavelet function, $\langle\rangle$ represents the inner product.

The SWT decomposition process is shown in Fig. 3. Single-level decomposition of an image into four coefficient images (A, H, V, and D) of the same size as the original image, where A, H, V, and D represent the low-frequency coefficients and the high-frequency coefficients in the horizontal, vertical, and diagonal directions, respectively. The low-frequency coefficients are used in the next level of decomposition.

In this paper, we perform 5-level decomposition on the downsampled fringe image, and 15 high-frequency coefficients and 1 low-frequency coefficient are obtained. The 5-level decomposition can effectively separate the fringes from the solar structure information. Less level decomposition will fail to separate these parts, and more level will waste time. Most of the fringes exist in the high-frequency vertical and horizontal coefficients, and a small part exists in the low-frequency coefficients and high-frequency diagonal coefficient. Therefore, in this paper, the wavelet coefficient is used as the input of neural network to remove the interference fringe and reduce the loss of solar structure information.

4. Network architecture

4.1. Data description

Deep learning methods require fringe-free images corresponding to fringe images, but they are difficult to obtain. Therefore, we adopt the method of superimposing the interference template on the fringe-free images to generate image pairs. We use these images as our dataset. We have 4000 pairs of images used as the training set and 1000 pairs for testing.

The fringe image size is 2160 × 2560, after rotation, it is 2432 × 2560. If the original image is not rotated, there will be obvious fringes in the horizontal, vertical and diagonal coefficient images after SWT decomposition. After rotation, the fringes will be concentrated in the horizontal and vertical coefficient images, while the diagonal coefficient images with only a small part of the data will have less obvious fringes. Since the Angle of the interference fringes in the Halpha image is almost constant, each image is rotated at the same Angle. The rotation Angle is manually selected. It is easier to extract interference fringe from rotating image.

We obtain the interference fringe template by stationary wavelet transform (SWT), band-stop filtering and Gaussian low-pass filtering. We perform 7-level SWT decomposition on the image. Most of the data have a relatively obvious fringe structure in the high-frequency vertical and horizontal coefficients of level 4, 5, and 6. Only a small portion of the data has less noticeable fringe in the high-frequency diagonal and low-frequency coefficients. We remove the interference fringes in the wavelet coefficients by band-stop filtering and Gaussian filtering. The parameters of filters are obtained by manually selecting the fringe region to obtain its spectrum and debugging. The fringes in the high frequency vertical coefficients are removed by means of Gaussian low-pass filtering and Butterworth band-stop filtering on the row data. The high frequency horizontal coefficient and the diagonal coefficient remove the fringes by the same method, but the horizontal coefficient is band-stop filtering for the column data, and the diagonal coefficient is band-stop filtering for the whole image. The low frequency coefficient is removed by Gaussian low-pass filtering. Then, we reconstruct the image by inverse stationary wavelet transform (ISWT). Finally, we take the residual of the fringe image and the reconstructed image as the fringe template. Fig. 4 shows the fringe template extraction result. We extracted 75 interference fringe templates by this method (The more templates the better, but due to time constraints we only got 75 samples. The time interval of the template is roughly the same across the 1794 stripe images because of some corrupted data, the time interval is different.). In addition, there are differences in the intensity of the interference fringe in each Hα image. By multiplying the intensity of the interference fringe

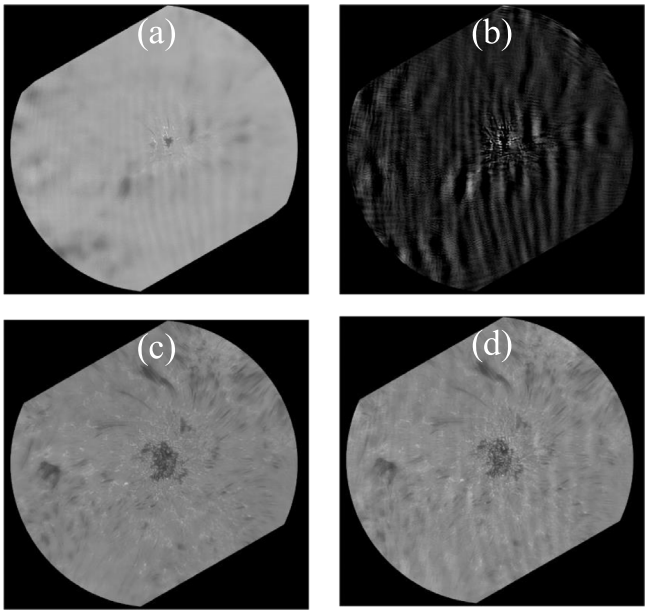

Fig. 4. (a) An Hα image with interference fringes that was obtained on 2014 August 13 at 17:52:01 UT. (b) The fringe sample obtained from (a). (c) An Hα image without interference fringes that was obtained on 2014 October 2 at 21:57:37. (d) Image of c superimposed with b.

template by 0.5, 1, 1.5, 2 and 2.5, we expanded the number of templates, and finally obtained 375 interference fringe templates.

4.2. Network architecture

The architecture of our network is shown in Fig. 5. Our method contains five steps: Gaussian pyramid, stationary wavelet transform, wavelet coefficient prediction, inverse stationary wavelet transform and Laplacian pyramid. The fringe image is first downsampled twice by a Gaussian pyramid. Then, the downsampled image is decomposed by stationary wavelet five levels to obtain wavelet coefficients. Then, the low-frequency coefficient of layer 5, the high-frequency vertical coefficients of layer 2, 3, 4 and 5, the high-frequency horizontal coefficients for each layer and the high-frequency diagonal coefficients of layer 2 and 3 are used as the input of the neural network. In addition, the residual learning strategy is used for model training. The residual obtained by subtracting the wavelet coefficients of the striated image and the nonstriated image was used as the learning target. After training, the model can indirectly learn the mapping relationship from fringe wavelet coefficients to fringe-free wavelet coefficients to remove interference fringes. Figs. 6 and 7 show the wavelet coefficients of the input and output of the neural network respectively. The prediction wavelet coefficients of network output are used to reconstruct the image by ISWT. Finally, the image size is recovered by Laplacian pyramid.

Our network model has 11 convolutional layers. All convolution kernel sizes are set to 5×5 and stride is set to 1. We pad zeros to ensure that the output of each layer has the same size. The number of kernels in the first 10 convolutional layers is set to 128. The number of kernels in the last convolutional layer is set to 12 to reconstruct the wavelet coefficients. The first layer is followed by a rectified linear unit (ReLU). Layers 2 to 10 are followed by batch normalization (BN) layers in addition to a rectified linear unit. Two bypass connection modules are set in the network, between layers 2 and 6 and between layers 6 and 10. In addition, the proposed model maps the wavelet coefficients of the fringe image to the residual wavelet coefficients of the fringe image and the fringe-free image through residual learning. Residual learning can reduce the difficulty of network learning features, and can solve the problem of gradient disappearance and gradient explosion to a certain extent (He et al., 2016). Our model takes the mean square error (MSE) of the network output wavelet coefficients and the residual wavelet coefficients as the loss function. The formula is as follows:

$$MSE\ (x_i, y_i) = (x_i - y_i)^2 \tag{2}$$

where x_i is the strip-free image and y_i is the model output image.

We use the adaptive moment estimation (ADAM) optimization method to minimize the loss function. The initial learning rate was 1×10^{-3} and then gradually attenuated until the 50th epoch with a learning rate of 1×10^{-4}. The network was trained for 50 epochs. We have 4000 pairs of images used as the training set. We used a single Nvidia RTX 3090 (24 GB) to train the network. The whole training phase takes about 44 h.

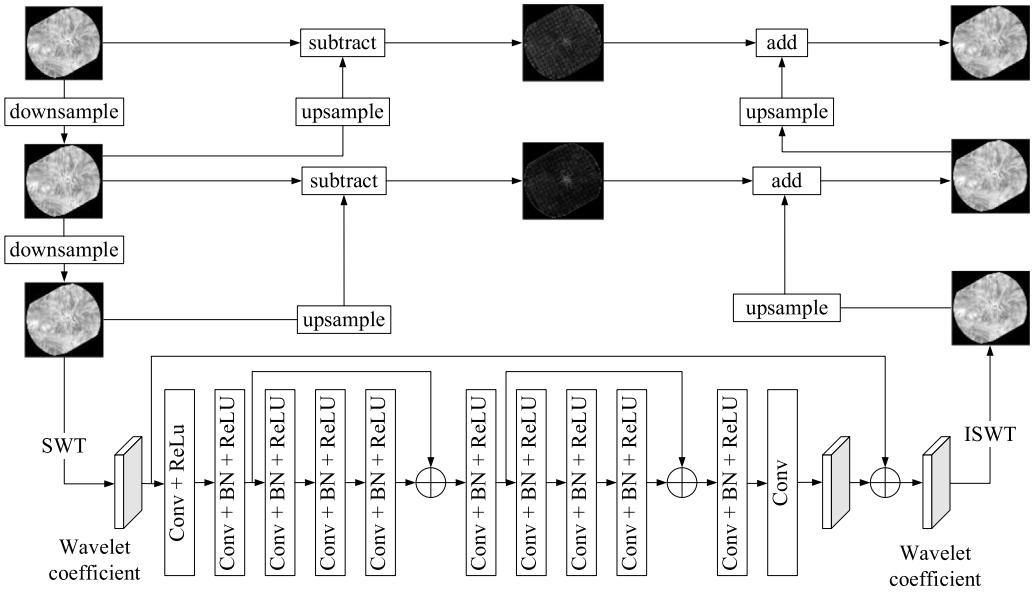

Fig. 5. Network structure. Our network consists of three parts: image pyramid, SWT and CNN.

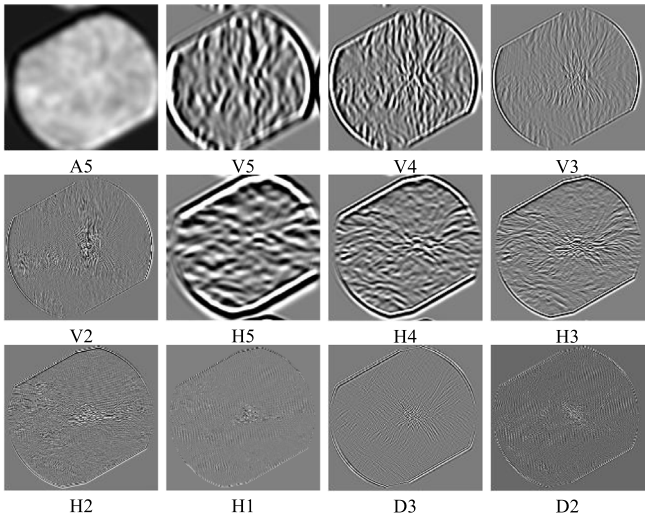

Fig. 6. The wavelet coefficients of the neural network input. Obvious fringe structure can be seen in the wavelet coefficient images.

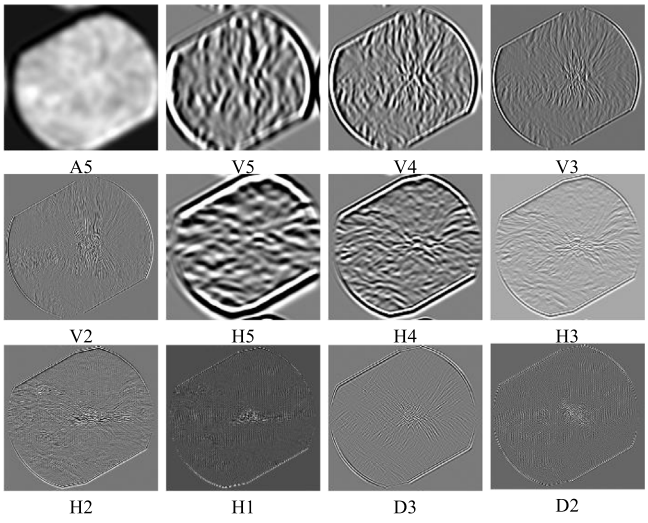

Fig. 7. The wavelet coefficients of the neural network output. Most of the fringes have been removed.

5. Experiments

5.1. Experiment with simulation data

We adopt the simulation data as test set to evaluate the performance of the de-fringe method and compare it with AWT, Gaussian high-pass filtering (GHPF) and DnCNN (He et al., 2014; Wang et al., 2016; Li, 2021). To objectively evaluate the removal effect of interference fringes, the peak signal-to-noise ratio (PSNR), mean absolute value (MAV) and multi-scale structural similarity (MS-SSIM, Wang et al. (2003)) are used to quantitatively describe the processing results of each algorithm. MS-SSIM is a modified version of SSIM. The performance of MS-SSIM is more stable and closer to the results of subjective evaluation. MAV, MS-SSIM is calculated as follows:

$$MAV = \frac{1}{M \times N} \sum_{i=1}^{M} \sum_{j=1}^{N} |y(i,j) - f(i,j)| \tag{3}$$

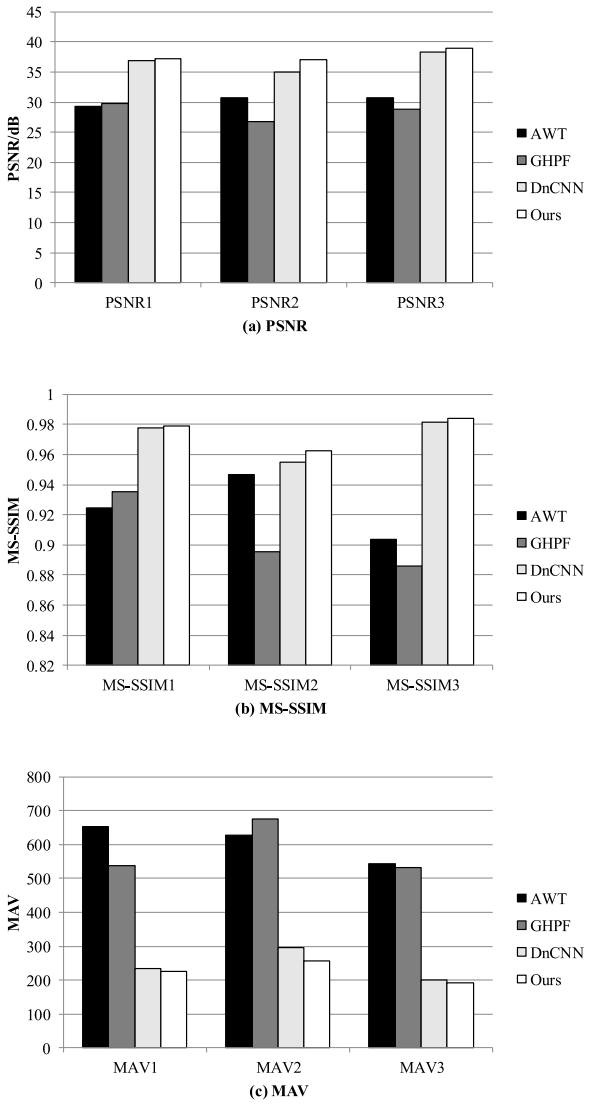

Fig. 8. PSNR, MS-SSIM and MAV comparison of different algorithm results.

$$\begin{cases} l(x,y) = \frac{2\mu_x\mu_y + C_1}{\mu_x^2 + \mu_y^2 + C_1} \\ c(x,y) = \frac{2\sigma_x\sigma_y + C_2}{\sigma_x^2 + \sigma_y^2 + C_2} \\ s(x,y) = \frac{\sigma_{xy} + C_3}{\sigma_x\sigma_y + C_3} \end{cases} \tag{4}$$

$$MS - SSIM(x,y) = [l_M(x,y)]^{\alpha_M} \cdot \prod_{j=1}^{M} [c_j(x,y)]^{\beta_j} [s_j(x,y)]^{\gamma_j} \tag{5}$$

$$C_1 = (K_1 L)^2, C_2 = (K_2 L)^2, C_3 = \frac{C_2}{2} \tag{6}$$

where M, N are the width and height of the image, $f(i,j)$ is the predicted value of the model and $y(i,j)$ is the true value of the sample, μ_x is the average of x, σ_x^2 is the variance of y, σ_{xy} is the covariance of x and y, $K_1 = 0.01$, $K_2 = 0.03$, M is the number of scales. In this paper, $M = 5$, $\alpha_1 = \beta_1 = \gamma_1 = 0.0448$, $\alpha_2 = \beta_2 = \gamma_2 = 0.2856$, $\alpha_3 = \beta_3 = \gamma_3 = 0.3001$, $\alpha_4 = \beta_4 = \gamma_4 = 0.2363$ and $\alpha_5 = \beta_5 = \gamma_5 = 0.1333$.

Fig. 8 shows the PSNR, MAV and MS-SSIM calculation results of the above methods, where the numbers after PSNR and MS-SSIM represent three different sets of data. The PSNR, MAV and MS-SSIM of our method and DnCNN are significantly higher than

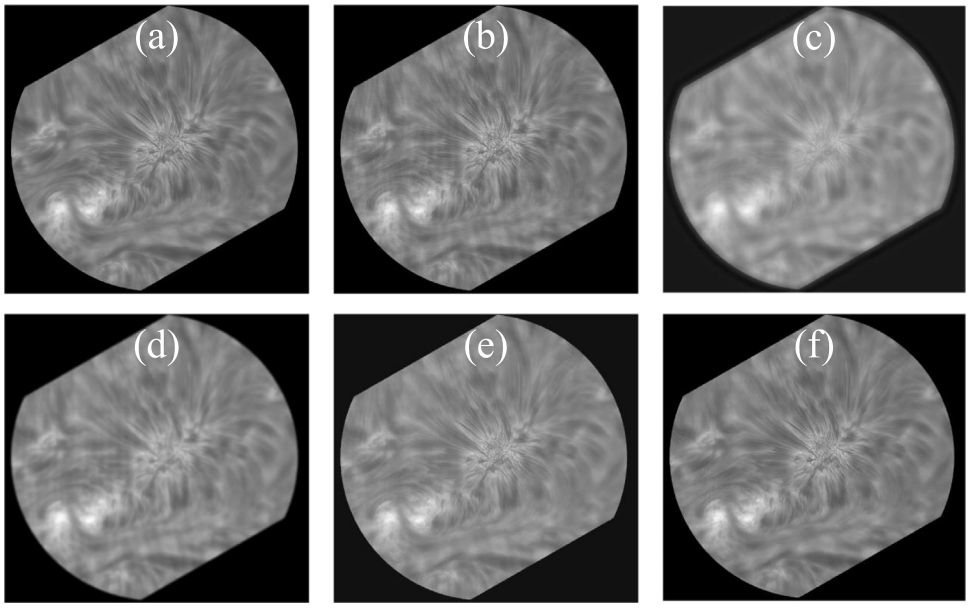

Fig. 9. Results of different methods on simulation data. (a) A fringe-free image, (b) the image obtained by superimposing the interference template on (a), (c) result of AWT, (d) result of GHPF, (e) result of DnCNN, and (f) our result.

Table 1
Evaluation results.

	DnCNN	Ours
Time	15,447 s	3145 s
PSNR	33.60	33.42
MS-SSIM	0.9588	0.9660
MAV	280	261

Table 2
Evaluation results of downsampled images.

	DnCNN	Ours
PSNR	36.00	38.89
MS-SSIM	0.9688	0.9779
MAV	267	244

those of AWT and GHPF. Our method also has better results than DnCNN. Fig. 9 illustrates the visual effects of the different methods. GHPF cannot remove the fringes and blurs the image. Although AWT can remove fringes, it will cause serious blurring of the image. DnCNN can remove most of the fringes, but some of them cannot be removed. Our method removes almost all the fringes and effectively preserves the solar structure.

In addition, the mean PSNR, MAV and MS-SSIM of DnCNN and our method on the whole test set and the time of model training for one epoch are shown in Table 1. The training speed of our model is significantly improved compared with DnCNN. The results of MAV and MS-SSIM were better than DnCNN. The results of PSNR is slightly lower than DnCNN. We also downsampled when using DnCNN, and the whole training phase takes about 10 days without sampling. Therefore, we also evaluated the downsampled images to compare the performance of SWT-CNN and DnCNN, and the results are shown in Table 2. Our method gives better results.

5.2. Validations on real fringe images

We further verify the effectiveness of the proposed method with Hα images with interference fringes obtained by GST. Since the methods of He and Wang were less effective, we only compared our method and DnCNN. The results are shown in Fig. 10.

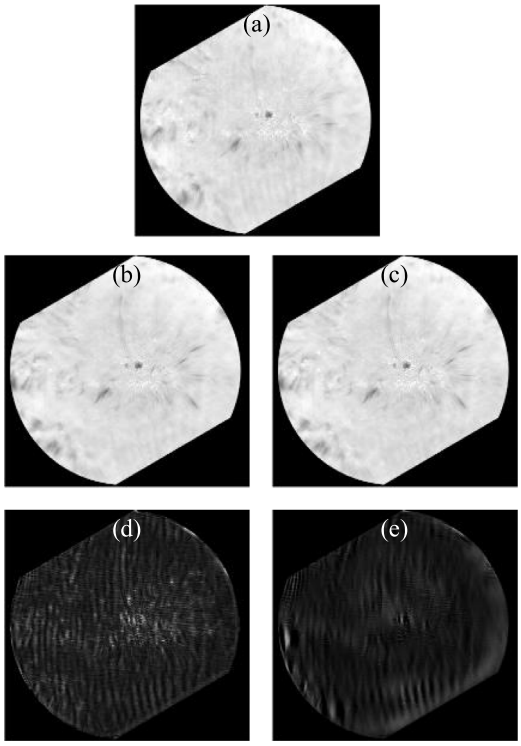

Fig. 10. Results of different methods on real fringe image. (a) The Hα image obtained by GST on 2014 August 13 at 16:59:05 UT, (b) the result of Li's method, (c) our result. (d) The residual of a and b. (e) The residual of a and c.

We obtain similar results on real data and simulated data. The result of DnCNN has more obvious interference fringe than ours. Therefore, our proposed method can truly and effectively remove the interference fringes in the Hα image. In addition, it can also be seen from Fig. 10 that (d) has more obvious solar structure information than (e). This means that our method can better preserve the solar structure information. Two other sets of results are shown in Figs. 10 and 11. In Fig. 10, there are fewer interference

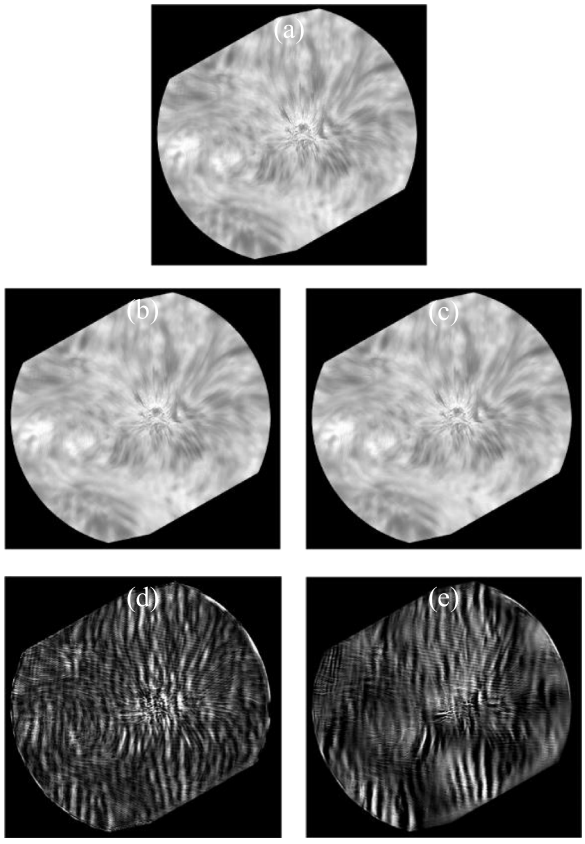

Fig. 11. Results of different methods on real fringe image. (a) The Hα image obtained by GST on 2014 August 13 at 17:39:07 UT, (b) the result of Li's method, (c) our result. (d) The residual of a and b. (e) The residual of a and c.

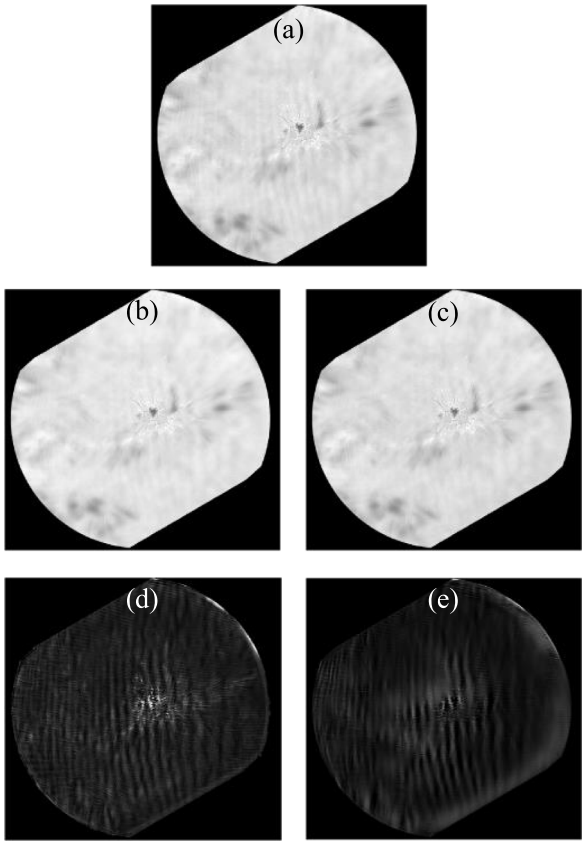

Fig. 12. Results of different methods on real fringe image. (a) The Hα image obtained by GST on 2014 August 13 at 17:54:05 UT, (b) the result of Li's method, (c) our result. (d) The residual of a and b. (e) The residual of a and c.

fringes in our results, but the advantage is not obvious, but it can be seen from the residual plot that the DnCNN results have a very obvious solar structure. As can be seen from Fig. 11, neither DnCNN nor our method can remove high-intensity interference fringes well (see Fig. 12).

6. Conclusions

To solve the problem of interference fringes in Hα images from the GST, this paper proposes a method that combines image pyramid and SWT-CNN model. The image pyramid accelerated network training speed, SWT-CNN utilizes the difference between interference fringe and solar structure in the frequency domain to remove interference fringes and retain solar structure information. The experimental results show that our proposed method can effectively remove the interference fringes in Hα images and preserve the solar structure. Reliable results are obtained both visually and quantitatively.

There are still some deficiencies in this paper. For the data with high fringe intensity, the fringe removal effect of our method is limited, which can remove most of the fringe, but the result still has relatively obvious fringe. While rotating the image makes it easier to remove streaks, it is also a limitation. In addition, the method of extracting the interference fringe template needs to be improved. As can be seen from Fig. 4(b), the fringe template we extracted contains obvious solar structure information, which leads to the removal of part of the solar structure as fringes in the learning process of CNN. At the same time, the number of stripe templates needs to be increased. The selection of parameters in the methods used in this paper is based on experience, so they are not optimal. Those limitations can be addressed on follow-up studies.

CRediT authorship contribution statement

Kui Wu: Conceptualization, Methodology, Software, Writing – original draft, Editing.

Declaration of competing interest

The authors declare that they have no known competing financial interests or personal relationships that could have appeared to influence the work reported in this paper.

Data availability

Data will be made available on request.

Acknowledgments

We gratefully acknowledge the use of data from the Goode Solar Telescope (GST) of the Big Bear Solar Observatory (BBSO). BBSO operation is supported by US NSF AGS-1821294 grant and New Jersey Institute of Technology. GST operation is partly supported by the Korea Astronomy and Space Science Institute and the Seoul National University.

References

Adelson, E., Anderson, C., Bergen, J., Burt, P., Ogden, J., 1983. Pyramid methods in image processing. RCA Eng. 29, 33–41.

Burt, P., Adelson, E.H., 1983. The Laplacian pyramid as a compact image code. IEEE Trans. Commun. 3, 532–540. doi:10.1109/TCOM.1983.1095851.

Cai, Y.F., Ji, K.F., Xiang, Y.Y., 2018. Extraction of solar spectral information based on principal component analysis. Spectr. Anal. 38, 2847–2852.

Gao, J.Z., Liu, Y., Bai, X., Zhang, Q., Gui, Z.Q., 2018. Stationary wavelet domain deep residual convolutional neural network for low-dose computed tomography image estimation. J. Comput. Appl. 38, 3584–3590. doi:10.11772/j.issn.1001-9081.2018040833.

Guan, J.T., Lai, R., Xiong, A., 2019. Wavelet deep neural network for stripe noise removal. IEEE N.a. 7, 44544–44554. doi:10.1109/ACCESS.2019.2908720.

He, K.M., Zhang, X.Y., Ren, S.Q., Sun, J., 2016. Deep residual learning for image recognition. In: IEEE Conference on Computer Vision and Pattern Recognition 2016. doi:10.1109/CVPR.2016.90.

He, S., Zheng, S., Huang, Y., 2014. Removing the stripe noises interference on the hα full-disk solar image based on multiscale transform. Appl. Mech. Mater. 596, 365–369. doi:10.4028/www.scientific.net/AMM.596.365.

Kim, W., Lee, J., Kang, M., Kim, J.S., Choi, J.H., 2022. Wavelet subband-specific learning for low-dose computed tomography denoising. PLoS One 17, e0274308. doi:10.1371/journal.pone.0274308.

Li, Q., 2021. NVST Interference Fringes Classification Recognition and Removal Based on Deep Learning (MA thesis). China Three Gorges University, doi:10.27270/d.cnki.gsxau.2021.000312.

Li, Y., Zheng, S., Huang, Y., Liu, D.J., 2019. An interference fringes removal method based on multi-scale decomposition and adaptive partitioning for nvst images. J. Korean Astron. Soc. 52, 49–55. doi:10.5303/JKAS.2019.52.2.49.

Liu, Z.S., Lai, R., Guan, J.T., 2022. Spatial and transform domain CNN for SAR image despeckling. IEEE Geosci. Remote. Sens. Lett. 19, 1–5. doi:10.1109/LGRS.2020.3022804.

Liu, D.J., Zheng, S., Huang, Y., 2020. NVST chromosphere data interference fringes removal based on NSCT and PCA. Astron. Comput. 30, 1–6. doi:10.1016/j.ascom.2020.100366.

Liu, D.J., Zheng, S., Huang, Y., Xiang, Y.Y., 2021. New vacuum solar telescope fringe removal based on Fringes flat field. Sol. Phys. 296, 28–37. doi:10.1007/s11207-021-01775-8.

Nason, G.P., Silverman, B.W., 1995. The stationary wavelet transform and some statistical applications. Wavelets Stat. 103, 281–299. doi:10.1007/978-1-4612-2544-7_17.

Wang, Z., Simoncelli, E.P., Bovik, A.C., 2003. Multi-scale structural similarity for image quality assessment. In: 37th Asilomar Conference on Signals, Systems and Computers, 2003. doi:10.1109/ACSSC.2003.1292216.

Wang, S.B., Xu, Z., Xiang, Y.Y., Jin, Z.Y., 2016. Study and removal of the interference fringes in images observed by the imaging system of nvst. Acta Astron. Sin. 57, 608–619. doi:10.15940/j.cnki.0001-5245.2016.05.010.

Zheng, S., He, S., Huang, Y., He, H.L., Lin, G.H., 2016. Automated removal of stripe interference in full-disk solar images. Res. Astron. Astrophys. 16 (6), 2. doi:10.1088/1674-4527/16/6/087.